Laser Ignition of Bulk Iron, Mild Steel, and Stainless Steel in Oxygen Atmospheres

Maryse Muller, Hazem El-Rabii, Rémy Fabbro

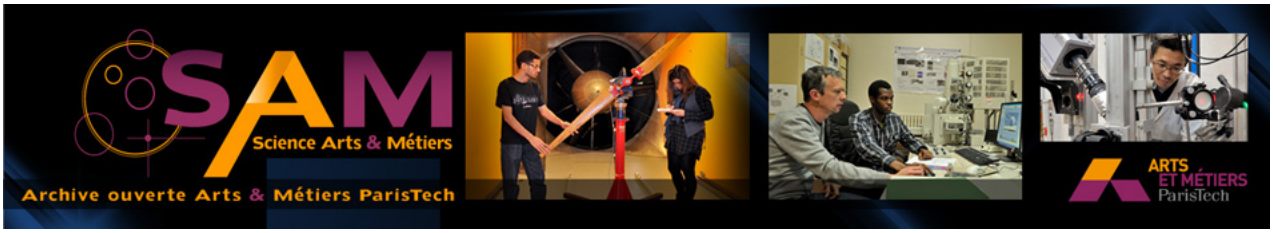

LASER IGNITION OF BULK IRON, MILD STEEL, AND STAINLESS STEEL IN OXYGEN ATMOSPHERES

Maryse Muller,[1−3] Hazem El-Rabii,[2] and Rémy Fabbro[3]

[1]*CRCD, Air Liquide, Jouy-en-Josas, France*

[2]*Institut Pprime, CNRS - ENSMA - Université de Poitiers, Futuroscope Chasseneuil, France*

[3]*Laboratoire PIMM, CNRS - Arts et Métiers ParisTech, Paris, France*

The ignition of pure iron, mild steel S355J, and stainless steel 316L has been investigated. The whole ignition and combustion processes have been monitored using a high-speed video camera and adapted pyrometry. Our results show that the absorptivity of the iron and mild steel to laser radiation increases rapidly at 850 K, from 0.45 to 0.7, and that of stainless steel increases more gradually during the heating process from 0.45 to 0.7. The ignition of iron, mild steel, and stainless steel is controlled by a transition temperature, at which the diffusivity of the metal increases sharply. The transition temperature of pure iron and mild steel is around 1750 K, when molten material appears, and that of stainless steel is around 1900 K, when the solid oxide layer loses its protective properties. These temperatures are independent of the oxygen pressure (from 2 to 20 bar) and of the laser intensity (from 1.6 to 34 kW·cm^{-2}). During ignition, the temperature increases very strongly at first, and after that a change in the heating rate of the surface is observed. A diffusive-reactive model, provided with equations describing the diffusion of oxygen in the metal and the transfer of heat released by the oxidation reactions has been solved. The model correctly reproduces the sharp rise of temperature as well as the decrease in the heating rate that follows. Comparison between calculated and experimental data shows that, without liquid convection flow in the melt, combustion would extinguish as soon as the metal surface is fully oxidized and that the combustion front moves into the metal.

Keywords: Combustion; Ignition energy; Iron; Oxygen; Steel

1. INTRODUCTION

The use of metals in high-temperature, high-pressure, and oxidizing environments encountered in many technological applications involves significant fire hazards. To ensure safety operation of systems working in such conditions, a reliable assessment of fire hazards is a prerequisite that requires an accurate knowledge of metal flammability properties.

Attempts to develop standard tests that identify the conditions under which a metallic material is considered as flammable have been made since the early 1970s (Neary, 1983). A review of the literature shows that the most popular standards are currently those

Address correspondence to Maryse Muller, CRCD, Air Liquide, 1 Chemin de la porte des Loges, Les Loges en Josas, 78354 Jouy-en-Josas, France. E-mail: muller.maryse@gmail.com

proposed by the American Society for Testing and Materials (S-A, 2003), the National Aeronautics and Space Administration (S-N, 1998), and the International Organization for Standardization (S-I, 2003). The purpose of these tests is to quantify the relative *flammability* of different metals, i.e., their relative propensity to *sustain* combustion of metallic materials of standardized dimensions in oxygen atmospheres. This material ranking is achieved by determining their pressure threshold, i.e., the pressure above which the combustion of a vertical cylindrical sample, after being initiated on its lower part—usually an electrically heated metal wire (Bolobov et al., 1992; Sato et al., 1983)—enters a self-sustained regime, leading to full or considerable destruction of the samples (McIlroy et al., 1988; Steinberg et al., 1989).

Such a testing configuration has, however, major drawbacks when applied to the study of the onset of ignition. First, the amount and localization of the energy actually transferred to the investigated metal are not reproducible, and only a poor estimate of its value can be obtained. Also, the reaction between the metal wire and the metallic sample may modify the kinetics of ignition. To overcome these two problems, non-intrusive techniques have been used to ignite the metallic samples. For instance, Bolobov et al. (1991, 1992) and Sato et al. (1995) used inductive heating. Focalized laser beams (Arzuov et al., 1979; Bransford, 1985; Kirichenko et al., 1989) or collimated xenon lamp beams (Branch et al., 1992; Nguyen and Branch, 1987) have also been used to ignite small bulk metallic samples, with intensities of approximately 1 $MW{\cdot}m^{-2}$. In spite of their obvious advantages over metal wires, as being highly reproducible, contactless, and controllable sources of energy, the low intensity of these light sources ($\sim 1MW \cdot m^{-2}$) leads to durations of the heating process very similar to those obtained with inductive heating (several seconds to several dozens of seconds). However, ignition sources involved in accidental metal fires are much shorter, and the very long heating duration used in these tests may imply considerable changes in the ignition conditions (e.g., oxidation state, global preheating of the whole sample).

In this article, we will be concerned with the onset of the combustion of bulk metals by means of intense (2–500 $MW \cdot m^{-2}$) and short (5 ms–1 s) laser pulses. The metals investigated here are mild steel (S355 - 0.2% carbon) and stainless steel (316L) due to their extensive use in oxygen supply systems. High-purity iron is also considered, as it provides a reference material for comparison with S355 and 316L. The specimens consist in cylindrical rods, which were ignited by focusing the laser beam on their top surfaces. The experimental approach provides time-resolved surface temperature, ignition temperature, and high-speed imaging of the heating, ignition, and combustion stages of the metal specimens.

The article is organized as follow. Section 2 is devoted to the presentation of the experimental set-up. In Section 3, we present and discuss our experimental results for pure iron and mild steel. In Section 4, a one-dimensional model for the ignition of pure iron is proposed and numerical results are discussed and compared to the associated experiments. In Section 5 we present and discuss our experimental results for stainless steel. Section 6 summarizes our conclusions.

2. EXPERIMENTAL SET-UP

A schematic of the experimental set-up for laser ignition of the metal rods is shown in Figure 1a. The cylindrical metal samples studied were 3.2 mm in diameter for mild steel and stainless steel, and 3 mm in diameter for pure iron, and 15 to 25 mm high. Prior to tests, the samples top surface were abraded with rough sandpaper to ensure a sufficient

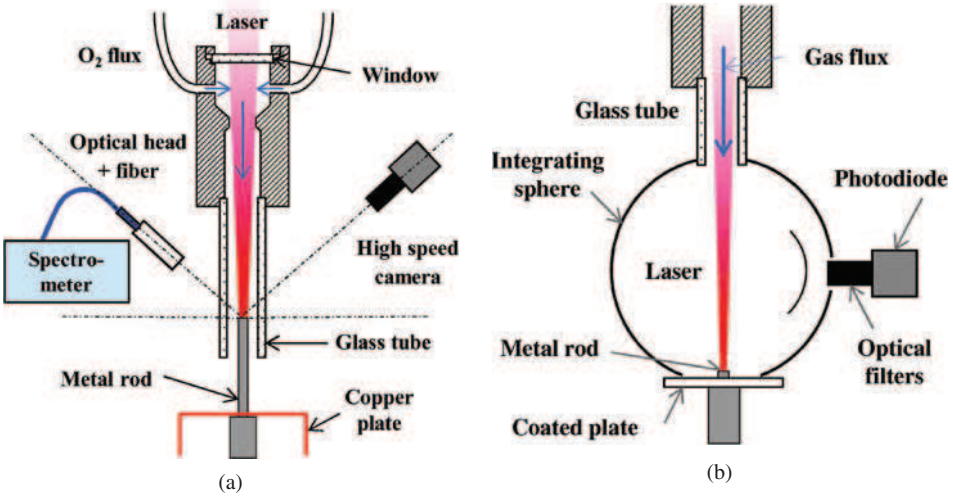

Figure 1 Schematics of (a) the rod ignition set-up with the optical pyrometry experimental set-up; (b) absorptivity measurement set-up.

and reproducible absorptivity to laser radiation. The samples were fixed in a small chuck and inserted into a borosilicate glass tube (with an inner diameter of 16 mm), transparent to radiation in the wavelength range from 500–1000 nm. Oxygen gas flowed out through the glass tube (at a flow rate of 40 $l \cdot min^{-1}$) providing an oxidizing atmosphere to sustain combustion. Most of the tests were conducted at atmospheric pressure.

The metal rods were heated up by a disk laser operating at 1030 nm (Trumpf, Trudisk 10002). The laser beam was delivered through an optical fiber with a core diameter of 600 μm, providing a spatially uniform intensity distribution that was imaged onto the top of the rod by a set of two lenses. The circular beam spot size so obtained was 3 mm in diameter, which ensured a homogeneous heating of the top surface of the rod.

Two different pyrometers were used to measure the top surface temperature of the rod during ignition and combustion: a 2D single-band pyrometer measured the energy being radiated in the 800–950 nm wavelength range with a high-speed video camera and a spectral pyrometer recorded radiations from 500–700 nm. Both pyrometers and their calibration are described in detail in Muller et al. (2012). The pyrometers axes were tilted 45° with respect to rod axis. For the spectral pyrometer, an imaging head with two achromatic lenses ensured the coupling between heat radiation emitted by a 0.6 mm diameter spot on the sample top surface and an optical fiber connected to a spectrometer. The camera, the spectrometer, and the laser were triggered by the same signal, ensuring synchronous data acquisition. Time $t = 0$ corresponds to the beginning of the laser pulse.

The set-up for the measurement of absorptivity of the metallic samples during laser heating under oxygen is shown in Figure 1b. The sample was placed at the bottom of an integrating sphere with $BaSO_4$ coating. The incidence angle was set at 10° in order to capture the first reflection from the sample within the sphere. A photodiode (with linear response with intensity in the power range used) was placed behind a small $BaSO_4$ coated sheet of metal, in order to ensure a sufficient number of reflections of light in the sphere before detection by the photodiode. The photodiode measures the laser intensity reflected at the top of the rod, and thus does not contribute to the heating up of the rod. A calibration factor k was determined using a small piece of metal coated with $BaSO_4$ in place of the rod

as a reference (reflectivity data at 1030 nm from data sheet: 97%). The absorptivity A of the top of the sample was deduced by the formula:

$$A = P_{\text{in}} V_{\text{r}}^{-1} k^{-1}, \tag{1}$$

where V_{r} is the signal from the photodiode and P_{in} is the laser power.

3. IRON AND MILD STEEL: EXPERIMENTAL RESULTS AND DISCUSSION

3.1. Heating and Oxidation in Solid State

The surface of the rod was observed using a fast camera during laser heating (Figure 2a). During the heating process, the surface darkens as can be seen from videos. The temperature of the rod was measured simultaneously using several type K thermocouples along the rod, at different distances from the surface. An example of the results obtained is

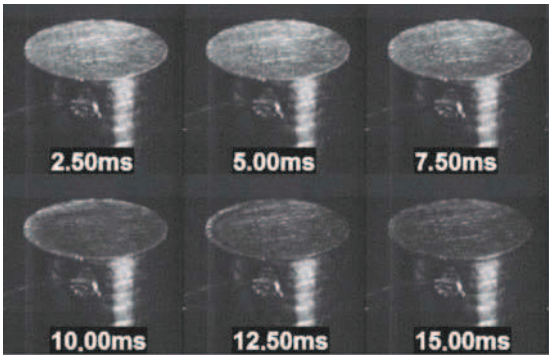

(a)

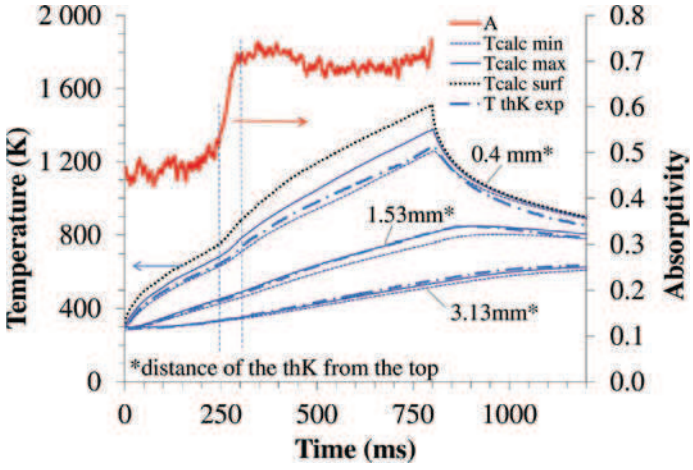

(b)

Figure 2 (a) Temporal evolution of the surface of a mild steel rod during laser heating in oxygen during laser irradiation of 1 kW; (b) temporal evolution of a mild steel rod absorptivity during laser irradiation of 180 W, and corresponding measured and calculated temperatures along the rod.

showed in Figure 2b: absorptivity (thick line) and temperatures at different distances from the top (thick dotted lines) are superimposed on the graph. For iron and mild steel, the transition from a low absorptivity (0.45) to a high absorptivity can be observed during the laser heating phase. This transition coincides with the darkening of the surface (Figure 2).

Seban (1965) reports an absorptivity of 35% for a pure, polished iron surface at 1123 K and at perpendicular incidence. Considering the roughness of the surface of our samples, the value of 45% that we found is realistic. Moreover, such a sharp rise in the absorptivity (at 1064 nm) from 0.4 to 0.7, for an oxidizing surface, was also reported by Seibold et al. (2000).

This abrupt change in absorptivity modifies the amount of energy transferred to the rod. Indeed, as one can see in Figure 2b, the rise in temperature, at 0.4 mm from the top surface, increases faster from 250 ms, that is, when the absorptivity increases sharply.

The solution of the 2D axisymmetric heat equation, supplemented by appropriate boundary conditions, was compared to the temperatures measured. The model of heat flow along a cylindrical rod with radius $r = 16$ mm, length $l = 20$ mm, density $\rho(T)$, specific heat capacity $c_p(T)$, thermal conductivity $k(T)$, and heat transfer coefficient h is given by:

$$\rho c_p \frac{\partial T}{\partial t} = \nabla \cdot (k \nabla T), \tag{2}$$

where t is time and T is temperature. The values of $k(T)$, $c_p(T)$, and $\rho(T)$ are those of mild steel S355 and were taken from Technique pour l'utilisation de l'acier (France) (1995); h was set to 10 $\mathrm{W{\cdot}m^{-2}{\cdot}K^{-1}}$.

The rod is initially at temperature T_0. Heat exchange with the surrounding medium (which is at temperature T_0) through the surfaces of the rod determines the boundary conditions. For the side and the bottom of the cylinder, they are given by

$$k\,(\boldsymbol{n} \cdot \nabla T) = h\,(T_0 - T), \tag{3}$$

where $\boldsymbol{n}$ is the outward unit normal vector to the cylinder surface.

The laser heating at the top surface yields the following boundary condition

$$k\,(\boldsymbol{n} \cdot \nabla T) = I_0\,(\boldsymbol{n} \cdot \mathbf{1}_z) + h\,(T_0 - T). \tag{4}$$

Here $\mathbf{1}_z$ is the unit vector in the upward direction and I_0 is the laser flux given by

$$I_0(T) = A_0(T)\,\frac{P}{S_r}, \tag{5}$$

where $S_r = \pi r^2$, $A_0(T)$ is the absorptivity at the top surface, and P is the time-averaged laser power. In our calculations, we took experimental values of $A_0(T)$.

For each thermocouple, the temperature has been calculated for two positions, corresponding to the upper and lower edges of the junction. As can be seen, the experimental temperature curves lies between the calculated curves for these position, showing that the assumed parameters $k_{th}(T)$, $c_p(T)$, and $\rho(T)$ are correct. The calculation of the surface temperature showed that the sharp rise in A_0 occurs when the surface reaches approximately 800 K. Such behavior has been observed repeatedly for any laser power from 180–2000 W. Seibold et al. (2000) also observed that the strong increase in the absorptivity of the sample from 0.4 to 0.7 occurred when the sample reaches 840 K.

When iron or mild steel oxidizes in oxygen atmospheres, a two- or three-layer scale of iron oxides forms at its surface. The number, composition, and oxide layer sequence depend on the temperature. At temperatures below 840 K, only Fe_2O_3 and Fe_3O_4 form. Above 840 K, the oxidation rate of pure iron strongly increases, and an additional layer of FeO forms next to the metal (Gemma et al., 1990). The rapid growth of the FeO layer above 840 K is responsible for the increase of absorptivity observed and for the increase in the laser heating rate. The contribution of the heat released by the oxidation reactions to the heating up of the surface can obviously be considered negligible when compared to the energy provided by laser heating.

3.2. Ignition

In the present work, we consider that ignition corresponds to the onset of an accelerated heating of the system caused by a substantial acceleration of the oxidation rate. The temperature at which this onset happens is called ignition temperature.

The temperature of the top surface of pure iron rods was tracked using a 2D monoband pyrometer during the laser heating process in oxygen leading to ignition with various laser power. Emissivity of the sample was assumed to be 0.7 when the temperature exceeds 840 K, in accordance with the absorptivity measurements mentioned above, considering that the value of emissivity of the sample at 45° in the range 800–950 nm can be approximated by the value of absorptivity at 1030 nm at normal incidence (Kirchhoff's law). Figure 3a shows the top surface temperature of mild steel rods during laser heating for various laser powers.

Each curve in Figure 3a can be divided into three parts, independent of the laser power used: (1) a linear part before ignition (stage A), (2) a linear part after ignition (stage B), which heating rate is always considerably greater, (3) a more irregular and less repeatable part with a lower heating rate (stage C). For all laser powers, ignition occurs when the surface reaches a temperature around 1650 K. This temperature is the ignition temperature of iron in our experimental conditions.

Pictures from video camera monitoring (Figure 4) showed that ignition occurs at the surface when molten material appears at the surface, independent of the laser power. The only difference between low laser power (Figure 4a) and high laser power (Figure 4b) is that the liquid appears more homogeneously on the surface for the latter than for the former. The ignition temperature of 1650 K corresponds to the melting point of FeO (Table 2). This temperature is close to the melting point of iron (1810 K) and mild steel (1713–1778 K). Given the fact that the diffusion rate is normally several orders of magnitude greater in the liquid than in the solid (Abbaschian et al., 2010), the increase in the diffusion rate induces a better mixing of the reactants and thus a greater rate of reactions in the liquid. The resulting greater heat release is responsible for the strong increase in the temperature, which, in turn, induces the formation of more liquid.

The value of 1650 K for the ignition temperature of iron or mild steel is the highest that can be found in the literature. Bolobov (2001) investigated the effect of the surface/volume ratio of the sample on the ignition temperature, and found that the ignition temperature of iron foils is 300 K lower (1233 K) than that of thicker samples (between 1523 and 1613 K). Similarly, Laurendeau and Glassman (1971), comparing their results to those of von Grosse and Conway (1958), showed that the heating rate has considerable influence on the ignition temperature. Von Grosse and Conway heated their samples under an inert atmosphere prior to exposing them suddenly to a flow of oxygen and found an

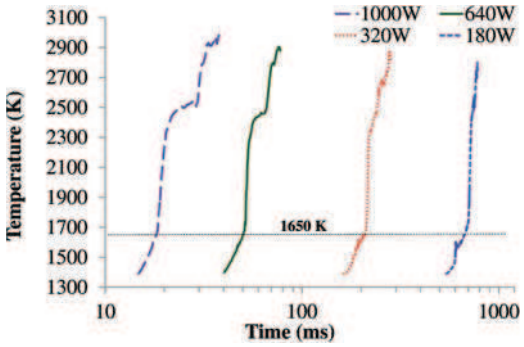

(a)

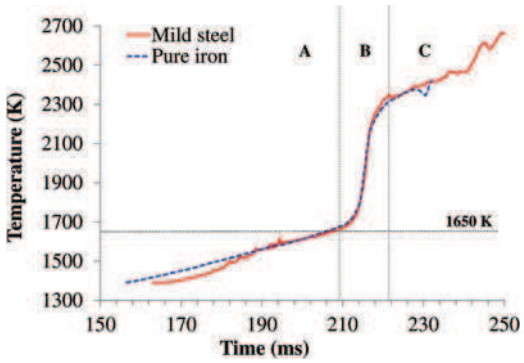

(b)

Figure 3 (a) Temporal evolution of the surface of a mild steel rod during laser heating in oxygen during laser irradiation with various powers; (b) comparison between iron and mild steel rod (laser pulse power of 320 W).

(a)

(b)

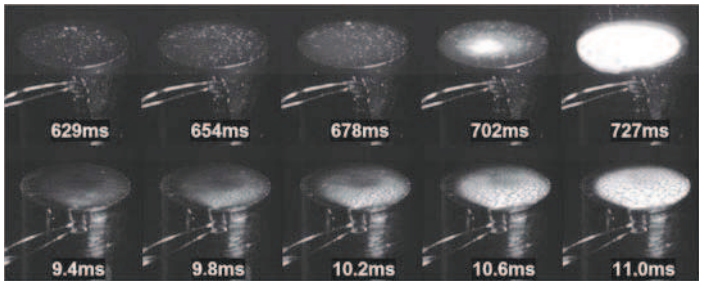

Figure 4 Top surface of a mild steel rod during laser ignition: (a) 180 W, (b) 1.5 kW.

ignition temperature of 930 K, while Laurendeau and Glassman heated slowly the samples in an oxygen atmosphere until ignition occurred, and found 1315 K. These discrepancies can be explained as follows: in Laurendeau and Glassman's experiment, the growth of surface oxide layer is small, the protective role of the oxide is negligible, and the rapid heating causes little heat losses by conduction and convection, resulting in a low ignition temperature; in contrast, in von Grosse and Conway's experiment, a significant part of the heat

Table 1 Melting, boiling, and dissociation point of iron, mild steel, and stainless steel and of the oxide most likely to form during combustion

	T_f (K)	T_v (K)	T_d (K)
Fe	1810[a]	3343[a]	–
S355	1713–1778[b*]	3023[b]	–
316L	1648–1676[b*]		–
FeO	1650[a]	–	3687[a]
Fe_3O_4	1870[a]	–	2257[c]
Fe_2O_3	–	–	1730[a]
$FeCr_2O_4$	2453 [a]	–	–
Cr_2O_3	2708[a]	–	4273[a]

[a]Lide (2007).
[b]Technique pour l'utilisation de l'acier (France) (1995).
[c]Wilson et al. (1997).
*$T_{\text{solidus}} - T_{\text{liquidus}}$.

Table 2 Experimental pulse duration Δt_{exp} for ignition and calculated pulse duration Δt_{calc} to heat up the surface to 1650 K (mild steel rods)

P(W)	Δt_{exp} (ms)	Δt_{calc} (ms)
180	700	826
320	210	260
640	51	65
1000	18	26.5
2000	5	7.75

produced by oxidation may be lost by convection and conduction before ignition occurs, and a thick protective oxide layer has time to form. For ignition to occur, this oxidized layer must lose its protective properties, which results in a higher ignition temperature. According to the classification of Mellor (1967), in the first case, ignition is controlled by a critical temperature (at which the heat release by solid oxidation exceeds the heat loss), whereas in the second case, ignition is controlled by a transition temperature, at which the protective oxide loses its protective properties (cracking or melting).

The fact that we found the highest value of the ignition temperature for all laser heating conditions means that, even for the lowest tested laser intensity (180 W, that is 2.2 incident kW·cm^{-2}, or 1.6 absorbed kW·cm^{-2}), the laser heating rate is such that heat released by oxidation in the solid is negligible in the ignition process compared to the energy supplied by the laser, and that ignition is controlled by a transition temperature corresponding to the melting of FeO.

Furthermore, we obtained comparable behavior on iron rods in a vessel chamber in an oxygen atmosphere at higher pressure (10 and 20 bar) supporting the proposed explanation, given the fact that the melting point of FeO does not change from 1 to 20 bar (Shen et al., 1993).

Very similar results were obtained for pure iron and mild steel, as can be seen from Figure 3b. The curve of pure iron has been shifted by −26 ms in order to match the curve of mild steel. The ignition temperature is the same for pure iron as for mild steel, and the slopes of the temperature curves are the same, except for the small variations occurring before ignition for mild steel. These correspond to very small sparkling spots on the surface, undergoing ignition before the whole surface ignites. Such spots have also been noticed by

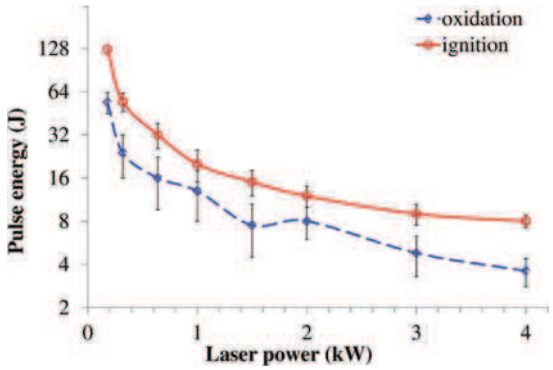

Figure 5 Incident pulse energy threshold of mild steel for apparition of dark oxide layer on the top and for ignition.

Sato et al. (1995) on bulk mild steel samples. Decarburization could be responsible for those igniting spots: careful observation shows that they are very small bubbles of liquid that burn, explode (probably due to CO formation), and then extinguish. Indeed, decarburization of mild steel resulting in the production of CO gas during oxidation is known to be responsible for the formation of blisters and micro-cracks during solid oxidation of mild steel (p. 231 Kubaschewski and Hopkins, 1962, p. 231), which leads to possible inhomogeneity in the surface temperature during laser heating, and thus local ignition.

We measured the incident laser pulse energy needed to ignite a mild steel sample (ignition threshold energy) for laser powers from 180 W to 4 kW, and we found that this energy decreases as laser power increases, as could be predicted from the heat transfer equation considering that the main heat losses are due to convective transfer (Figure 5). Incident laser energies needed to ignite 3.2 mm diameter mild steel rods are 5.6 to 90 absorbed joules or 8 to 130 joules of incident laser energy for laser powers from 4 kW to 180 W.

The simple model (described above) has been solved for various laser powers. The experimental pulse durations corresponding to ignition threshold are compared with the calculated pulse durations needed to heat the surface up to 1650 K as shown in Figure 1, considering that the absorptivity of the surface is 0.45 below 840 K and 0.7 above. Our model overestimates the durations by 20–30%. This could be due to particular thermophysical properties of the oxide surface layer, which are not taken into account in the model, and that could act as an insulating layer, at the same time increasing the heating rate and decreasing the heat transfer in a thin layer on the top.

The comparison between calculations based on the heat transfer equation and our experimental data shows that, before ignition (in our configuration with bulk iron samples), the decrease of the ignition energy threshold only depends on conductive thermal losses in the rod, and that the heat released by the oxidation in solid state can be neglected compared to the laser energy input.

3.3. After Ignition of Pure Iron and Mild Steel

As can be seen in Figure 3a and 3b, ignition of iron and mild steel is characterized by a very steep slope of the time-temperature curve of the surface of 10–20 ms (stage B), after which the heating rate decreases (stage III). This transition of the heating rate from stage B to stage C can be observed for all laser powers considered from 320–2000 W (open circles

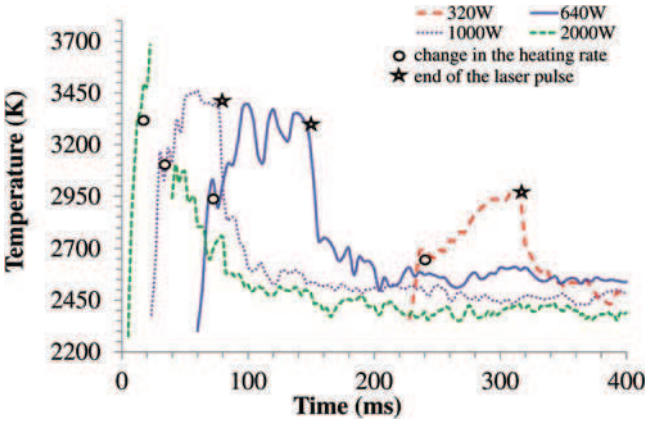

(a)

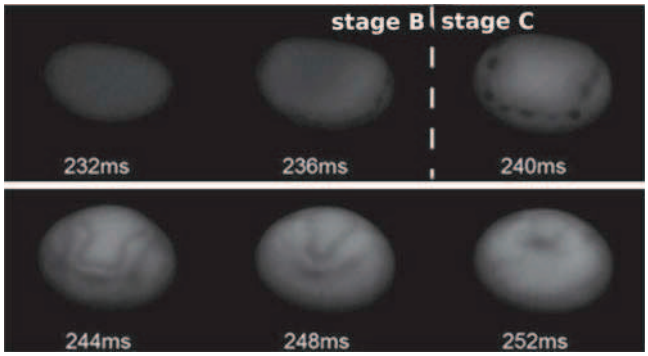

(b)

Figure 6 (a) Temporal evolution of temperature on the top surface of a pure iron rod during laser heating (laser 320 W); (b) corresponding infrared images.

Table 3 Surface temperature at the change of the heating rate depending on the laser power

P (W)	T_c (K)
320	2680
640	2900
1000	3150
1500	3240
2000	3300

in Figure 6a), but occurs at a temperature T_c increasing with laser power (see Table 3). Transition from stage B to stage C also corresponds to the formation of darker phases on the edges of the liquid, as can be seen from Figure 6b ($t = 240$ ms), which move on the surface from edges to the center ($t = 240$–252 ms).

Two explanations may be suggested concerning the transition from stage B to stage C. When the liquid reaches the edges of the rod, the thickness of the liquid increases, and convection movements start. This may cause changes in the heat transfer conditions.

Another explanation would be that, after the melting of the whole surface of the rod and after 10 or 20 ms, liquid iron at the surface is fully oxidized, so that the oxygen must then diffuse through the iron oxide layer to react with unoxidized iron into the melt, resulting in a decrease of the reaction rate.

4. 1D THERMO-CHEMICAL COMBUSTION MODEL

4.1. Description of the Model

To assess the validity of the second hypothesis, a system of equations describing the diffusion of the chemical species, their reaction inside a laser heated 1D iron sample, and the heat release corresponding to the oxidation reactions, as well as the diffusive heat transfer in the rod, has been formulated and solved numerically.

We have considered the simple following reaction between iron and oxygen:

$$\mathrm{Fe} + \mathrm{O} \rightarrow \mathrm{FeO}, \tag{6}$$

occurring within the metal according to an Arrhenius law, where A is the pre-exponential factor and E_a the activation energy, the local reaction rate being proportional to the concentrations C_O and C_F of each reactant. The local reaction rate inside the metal is given by:

$$S = C_O \; C_F \; A \; \exp\left(-\frac{E_a}{RT}\right), \tag{7}$$

where R is the universal gas constant.

The concentration of mono-atomic oxygen available at the top surface of the rod was considered constant. Oxygen and iron diffuse inside the metal according to Fick's law:

$$\frac{\partial C_O}{\partial t} - \frac{\partial}{\partial x}\left(D_O \; \frac{\partial C_O}{\partial x}\right) = -S, \tag{8}$$

$$\frac{\partial C_F}{\partial t} - \frac{\partial}{\partial x}\left(D_F \; \frac{\partial C_F}{\partial x}\right) = -S, \tag{9}$$

where D_O and D_F are the diffusivities of oxygen and iron in the sample, and S accounts for the consumption of reactants. Diffusivity D_F of iron is assumed to be zero, while diffusivity of oxygen D_O was considered the same in iron and in iron oxide, and such that:

$$\begin{array}{ll} D_O = 0 & \text{when} \quad T < 1800 \text{ K} \\ D_O = D & \text{when} \quad T \geq 1800 \text{ K}. \end{array} \tag{10}$$

A volumic heat source Q was introduced into the heat equation to take into account the heat released by the oxidation reactions:

$$\rho \; c_p \; \frac{\partial T}{\partial t} - \frac{\partial}{\partial x}\left(k_{th} \frac{\partial T}{\partial x}\right) = Q = S_q, \tag{11}$$

where q is the formation enthalpy of FeO in reaction (6). Here, the parameters k_{th}, ρ, and c_p were assumed to be independent of temperature, and the latent energy of fusion at the solid–liquid transition of iron occurring at 1810 K was neglected.

A progressive mesh was chosen to model the sample (2 cm long straight line): the distance between two nodes is 2 μm on the upper laser heated surface extremity ($x = 0$) and 200 μm on the other side ($x = x_{max}$).

The boundary conditions were:

$$\begin{array}{lll} C_O = 0 & \text{when} & T < 1800\ \text{K} \\ C_O = C_{Os} & \text{when} & T \geq 1800\ \text{K} \end{array} \quad \text{at } x = 0, \tag{12}$$

$$T = T_0 \text{ at } x = x_{\max}, \tag{13}$$

$$\frac{\partial T}{\partial x} = -\frac{I_O}{k_{th}} \text{ at } x = 0, \tag{14}$$

and I_0 is the laser intensity at the surface such as:

$$\begin{array}{ll} I_O = A_O(T)\ P/S_r & \text{when } t < \Delta t_{las} \\ I_O = 0 & \text{when } t \geq \Delta t_{las} \end{array}, \tag{15}$$

where $A_0(T)$ was set to a constant value of 0.7 and k_{th} is the thermal conductivity of iron. The power P and the duration of the laser pulse Δt_{las} is the duration of the laser pulse.

Initial conditions of the model were:

$$T(x; t = 0) = T_0 \text{ for any } x, \tag{16}$$

$$C_O(x; t = 0) = 0 \text{ for } x \neq 0, \tag{17}$$

$$C_F(x; t = 0) = C_{Fs} \text{ for any } x. \tag{18}$$

where C_{Fs} is the concentration of iron in pure solid iron, and C_{Os} is that of free unreacted oxygen in the melt. Data of the solubility of oxygen in liquid iron oxide are rare. We considered that the solubility of oxygen in liquid iron oxide is similar to that in liquid iron. Distin et al. (1971) gives, for atmospheric pressure of oxygen and at 2250 K, a molar ratio oxygen/iron of approximately 3%. Extrapolating from his results at 2770 K, we found a value of 10%, and we thus fixed the value of C_{Os} at approximately 10% of C_{Fs}. The values of the parameters used for calculations are given in Table 4.

4.2. Results and Discussion

As for experimental results, three stages, which we called stages I, II, and III can be distinguished on the calculated curves of the reaction power Q from surface to depth of the 1D sample for increasing times (Figure 7a) and on the curve of the integrated reaction power $\int_{-\infty}^{0} Q\, dx$ over time (Figure 7b). During stage I, the rod is heating up; the diffusivity of oxygen is low: oxygen remains on the surface, and the reaction rate is low everywhere in the sample. Stage II begins when the temperature reaches 1800 K on the top:

Table 4 Values of the parameters for the 1D thermo-chemical diffusion-reaction model

	Value	Units
q	256×10^3	$J{\cdot}mol^{-1}$
M_{FeO}	72×10^{-3}	$kg{\cdot}mol^{-1}$
c_p	400	$J{\cdot}kg^{-1}{\cdot}K^{-1}$
C_{Os}	1.00×10^4	$mol{\cdot}m^{-3}$
C_{Fs}	1.34×10^5	$mol{\cdot}m^{-3}$
A	0.4 – 20	$mol^{-1}{\cdot}m^{-3} \cdot s^{-1}$
E_a	$55 \times 10^{3*}$	$J{\cdot}mol^{-1}$
D	$10^{-8} - 10^{-6}$	$m^2{\cdot}s^{-1}$
ρ	7.5×10^3	$kg{\cdot}m^{-3}$
k_{th}	40	$W{\cdot}m^{-1} \cdot K^{-1}$
T_0	293	K

*Bolobov et al. (1992).

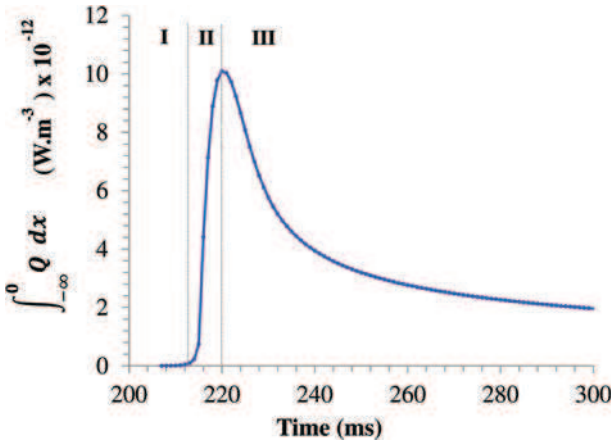

(a)

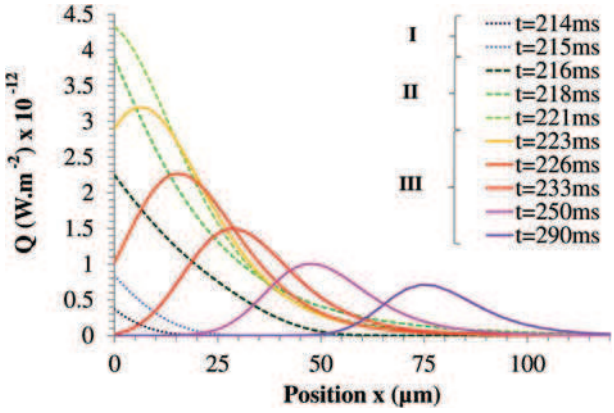

(b)

Figure 7 (a) Local chemical power Q depending on length x for different times; (b) chemical power Q integrated over the whole domain depending on time ($A = 4$ et $D = 6.3 \times 10^{-7}$ $m^2 \cdot s^{-1}$) and laser pulse of 320 W − 320 ms).

diffusivity of oxygen increases, oxygen and iron are mixed in the sample, and the reaction rate increases sharply, with a maximum on the surface, where concentrations of iron and oxygen are maximum. After full oxidization of iron on the surface, a stage III follows, where the reaction rate on the surface is zero, and the reaction zone penetrates into the sample. As oxygen diffuses, the maximum oxygen concentration penetrates deeper, and its value decreases, in accordance with Fick's law. The global chemical power $\int_{-\infty}^{0} Q\, dx$, depending on the concentration of oxygen, decreases strongly while oxygen continues to diffuse deeper into the sample.

Considering the above description, theses stages could be understood, respectively, as a laser heating phase (stage I), ignition (stage II), and propagation/extinction (stage III).

4.3. Influence of *A* and *D* Values on the Model

The model was tested for different combinations of the parameters A and D. We found that values in a range from 0.4–20 gave plausible results. Values of the diffusivity of oxygen in iron or iron oxide show very high variance in the literature. Li et al. (2000) reports discrepancies up to two orders of magnitude for D, depending on the experimental set-up used for measurement and the saturation in oxygen of the iron used. Li et al. (2000) also determined a value of the diffusivity of oxygen in an iron oxide layer in equilibrium with air at atmospheric pressure, of 4.2×10^{-7} $m^2 \cdot s^{-1}$ at 1888 K. Lower and higher diffusivities were tested in this model around this value, from 10^{-8} to 10^{-6} $m^2 \cdot s^{-1}$. The sensitivity of the model to these two parameters was assessed, and the influences of A and D on the surface temperature were investigated, and are presented in Figures 8a and 8b.

As for the curves of chemical power Q, the calculated temperature curves can be divided into three parts, corresponding to the three stages I, II, and III.

During stage I, the diffusivity of oxygen is almost zero, oxygen and iron do not mix, and thus no reaction occurs: variations of A and D do not affect this stage, and the heating of the surface is only due to the laser. At $T > 1800$ K, D_O increases, resulting in a strong increase of the reaction rate (stage II), and thus surface temperature. The general shape of the curve during stages II and III depends considerably on A: lower values of A induce longer durations of stage II, as well as reduced slopes during stage II, and a slower transition between stage II and stage III. On the contrary, D values only affect the final temperature level at the surface at the end of stage II and the duration of stage II, not the slope of the heating rate.

When full consumption of iron at the surface is accomplished, stage III occurs. The evolution of surface temperature during stage III is not affected by changes in A or in D. The heating rate is very similar to that of stage I, showing that, during this stage, heating is primarily due to the laser, and that the heat released inside the sample while the reaction zone penetrates deeper into the sample contributes negligibly to the surface temperature increase.

To summarize, parameter A controls the rate of reaction, and thus the thickness of the reaction zone: higher values of A result in more rapid reactions and quicker consumption of the reactant, inducing thinner reaction zones. Parameter D controls the diffusion of oxygen, i.e., the mixing between iron and oxygen in the sample. When D increases, oxygen goes deeper into the sample and the total number of reactions before extinction increases, as does the final temperature.

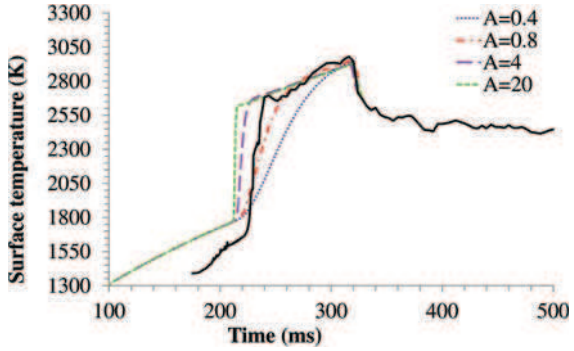

(a)

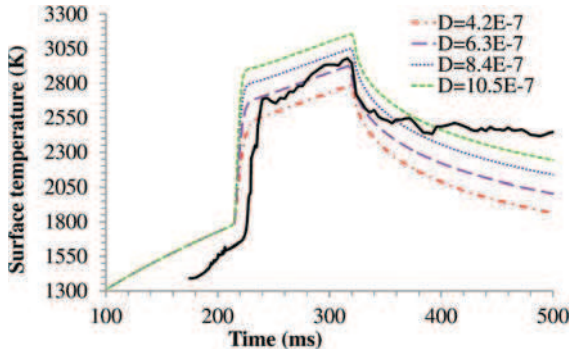

(b)

Figure 8 Experimental and calculated surface temperature of the rod ($x = 0$): (a) for $D = 6.3 \times 10^{-7}$ m$^2 \cdot$ s^{-1} and different values of A; (b) for different laser pulses and for $A = 4$ mol$^{-1} \cdot$ m$^3 \cdot s^{-1}$ et $D = 6.3 \times 10^{-7}$ m$^2 \cdot$ s^{-1}.

4.4. Discussion on the Comparison Between Experimental and Calculated Results

The values $A = 4$ mol$^{-1} \cdot$ m$^3 \cdot$ s^{-1} and $D = 6.3 \times 10^{-7}$ m$^2 \cdot$ s^{-1} give satisfactory agreement between calculated and measured temperatures over time, for different laser ignition pulses (Figure 9), except for a laser power of 180 W, for which the experimental transition from stage B to C is not correctly reproduced. Considering the good agreement between the experimental and calculated results, an identification of experimental stages A, B, and C and stages I, II, and III of the calculated results is attempted. The calculated results are in good agreement with the experimental results, and can provide a possible explanation of the physical mechanism involved.

Stage I, corresponding to laser heating before ignition, does not perfectly reproduce stage A; the heating rate is underestimated by the model. This could be due to the thermal insulating properties of the oxide layer at the surface, as already proposed to explain the discrepancies in the results of Figure 1. However, stage A and I are qualitatively similar: the solid rod is heated by laser, and no exothermic reaction occurs.

Stage II, corresponding to ignition, is caused by an increase in the diffusivity of oxygen above 1800 K, causing a steep rise in the reaction rate. We showed that experimental ignition is obtained when a transition temperature of 1650 K is reached: at this temperature

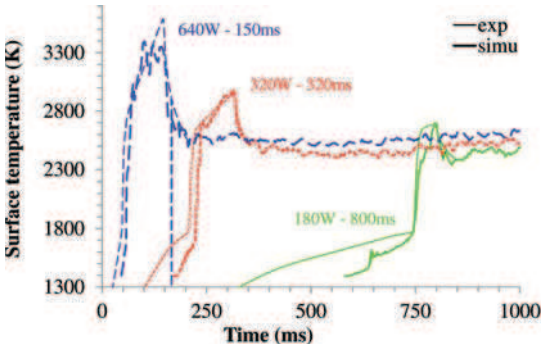

Figure 9 Experimental and calculated surface temperature of the rod ($x = 0$) for $A = 4$ mol$^{-1}\cdot$ m$^3 \cdot$ s^{-1} and $D = 6.3 \times 10^{-7}$ m$^2 \cdot$ s^{-1}.

liquid appears on the surface. Identification of stage II and stage B would lead us to infer that ignition is due to the increase of diffusivity of oxygen at the surface when liquid appears. Interestingly enough, in our model, the rate limiting mechanism of combustion during stage II is not diffusion, but the reaction rate. An objection could be made that in actual fact, oxygen is made available at the surface by an adsorption-dissociation process, which was not taken into account in the model, and could be the rate limiting mechanism during ignition. However, our results show that diffusion is not in any case the rate limiting mechanism during ignition.

In the model, the transition between stages II and III occurs when all the iron on the surface is oxidized, and corresponds to a transition from a regime where the oxidation reaction is the rate limiting mechanism to a regime where oxygen diffusion is the rate limiting mechanism. We can infer from those observations that the transition between stage B and stage C might involve a certain depletion in iron at the surface. Prior to this depletion, the rate limiting mechanism is probably the adsorption of oxygen on the surface or the reaction rate. When the depletion of iron occurs, the mixing of iron and oxygen might become the rate limiting mechanism, whether by diffusion or by flow convective movements.

Despite continuous heating of the surface by the laser, the global oxidation rate decreases during stage III, whatever the combination of A and D, so that self-sustained propagation of the combustion reaction was never obtained in the simulations, but on the contrary, extinction always began at the end of the laser pulse.

Propagation of the combustion would imply that the global chemical power increases or levels off, while the reaction zone penetrates deeper into the sample. Yet, the equations we used to model the chemical power Q [Eqs. (7) and (11)] show that an increase in Q could only come from either an increase in both reactants concentrations, or from an increase of the pre-exponential factor of the Arrhenius law A. However, the results indicate that, for all parameters tested, the pre-exponential factor of the Arrhenius law was never enough to compensate for a low concentration of iron or oxygen. Moreover, the diffusivity of oxygen was assumed to be constant above 1800 K, so that as the oxide layer grows, it makes the diffusion of oxygen and the contact between reactants more and more difficult; heat losses by thermal conductivity then progressively cause cooling and extinction of the rod.

However, one can see from the experimental results that, as soon as the laser stops, the temperature of the melt levels off at approximately 2400 K rather than decreases. In this simple thermal model, convection in the melt was not taken into account. A more accurate

model including fluid flow in the molten metal would allow us to determine the influence of the mixing of reactants induced by the convection movements on the combustion process.

5. STAINLESS STEEL: EXPERIMENTAL RESULTS AND DISCUSSION

The ignition of stainless steel rods was investigated as for iron and mild steel, using adapted pyrometer and absorptivity measurement. Contrary to pure iron and mild steel, for which the oxide formation occurs quickly when the surface reaches approximately 850 K, the oxidation of laser-heated stainless steel leads to a quasi-linear increase of absorptivity over time from 0.45 to 0.75 (Figure 10).

The energy threshold for the ignition of stainless steel was measured for lasers power from 180 to 4 kW, as well as the energy threshold for the formation of a visible oxide layer on the surface (Figure 11a). A very similar tendency to pure iron and mild steel was observed: the ignition threshold decreases as laser intensity decreases. For all laser intensities, the energy required to ignite stainless steel is roughly 1.5 times higher than of that of mild steel, i.e., 7 to 110 absorbed joules or 10 to 160 joules of incident laser energy for laser power of 4 kW to 180 W.

We also tracked the evolution of the surface temperature during the laser heating process (Figure 11b), and observed that ignition is controlled by a transition temperature of 1900 K, independent of the laser heating process. However, contrary to pure iron and mild steel, three different transition temperatures clearly appeared during the whole process: 1700 K, 1900 K, and 2300 K.

Indeed, the observation of the ignition process using high speed 2D videos revealed that, especially for low power laser pulses (180 to 640 W), when the surface reaches approximately 1700 K, wrinkles appear on the surface of the oxide layer (pictures b and c in Figure 12b) together with inhomogeneities in the surface temperature between the lower parts (valleys) and the upper parts (ridges) of the wrinkled oxide layer (Figure 12a). However, ignition does not occur until 1900 K is reached on the oxide layer. Because of the irregular texture of the oxide layer, ridges heat up more rapidly than valleys, and there is a delay between the ignition of the ridges (picture e of Figure 12b) and that of the valleys (picture f of Figure 12b). Contrary to mild steel and pure iron, the surface of the sample remains solid during the ignition process. Liquid, or partially liquid phases, appear on the surface only when temperature exceeds 2300 K (pictures f and g of Figure 12b).

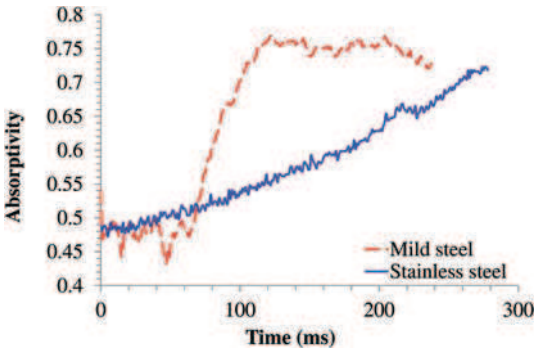

Figure 10 Absorptivity over time of a stainless steel and a mild steel rod during laser heating (320 W).

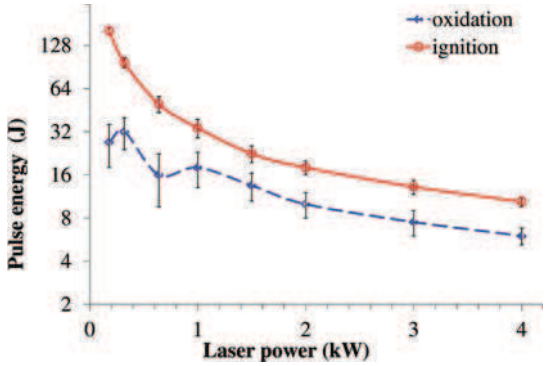

(a)

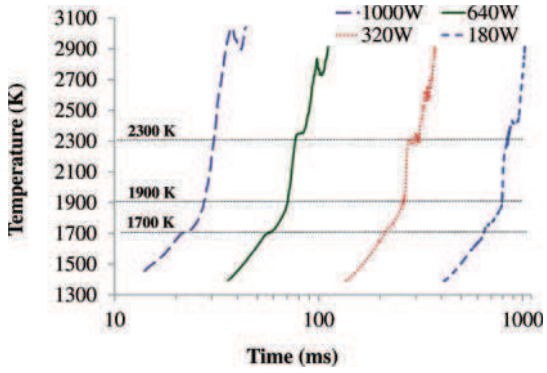

(b)

Figure 11 (a) Incident pulse energy threshold of stainless steel for apparition of dark oxide layer on the top and for ignition; (b) temporal evolution of the top surface of a mild steel rod during laser heating in oxygen (various laser powers).

An interpretation of the above description can be attempted, based on the structure of the oxide layer forming in isothermal conditions given by Moreau (1953), and on the melting point of the main oxides that may form in the process (Figure 13).

According to Moreau (1953), the oxide forming on the surface of a stainless steel sample from 1070 to 1520 K is mainly composed of a mixture of Fe-Cr spinel and magnetite Fe_3O_4, above a FeO layer with chromite $FeCr_2O_4$ inclusions, covered by a thin layer of Fe_2O_3. The melting of stainless steel and FeO occurs around 1700 K (see Table 2), as well as the dissociation of the Fe_2O_3 layer, implying that the upper oxide layer loses its mechanical support, which could explain why wrinkles appear on the surface while the upper solid oxide layer continues to grow. From that point on, the ridges of the wrinkles begin to be heated up by the laser more rapidly than the valleys. However, according to the relatively weak temperature increase from 1700 to 1900 K, we can infer that the solid upper oxide layer retains effective enough protective properties, and that reactions have thus negligible contribution in the heating of the surface below 1900 K.

At 1900 K, ignition occurs, and the temperature increases strongly, while the upper layer remains solid. This might correspond to the melting point of Fe_3O_4, according to Kubaschewski and Hopkins (1962) (Table 2). As can be seen from Figure 13, the protective

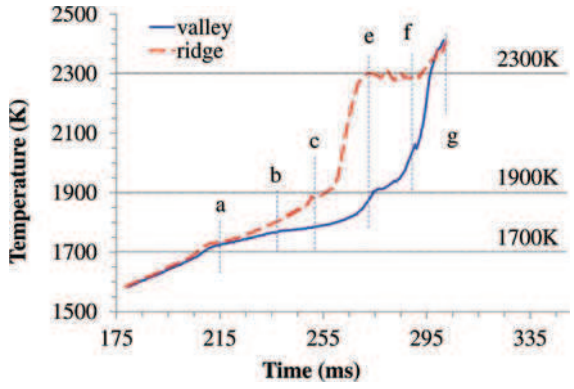

(a)

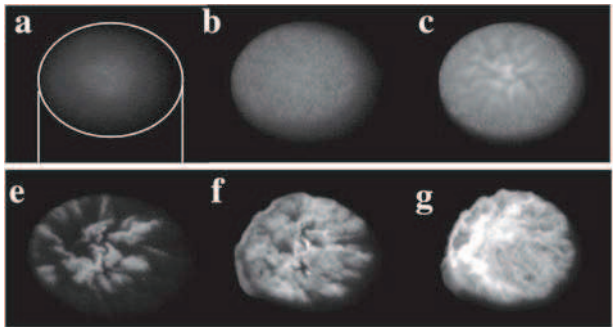

(b)

Figure 12 (a) Temporal evolution of temperature on two points of the top surface of a stainless steel rod during laser heating; (b) corresponding infrared images (laser 320 W).

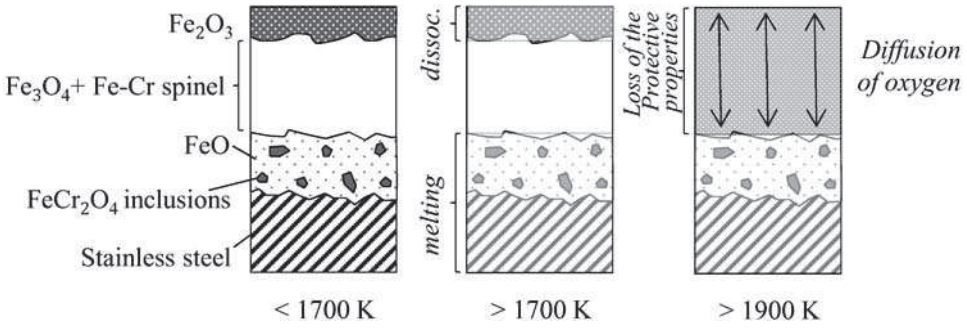

Figure 13 Proposition for an ignition process of laser heated stainless steel rod, based on a scheme on the isothermal oxidation from Moreau (1953).

oxide layer would be made of a mix of Fe_3O_4 and Fe-Cr spinel, according to Moreau (1953). Selective melting of Fe_3O_4 would result in the layer becoming porous, and then losing its protective properties. Oxygen might then diffuse through the oxide to reach the liquid steel underneath, inducing a strong increase in the oxidation rate, causing ignition.

After ignition, occurring at 1900 K, a porous spinel or chromite $FeCr_2O_4$ layer remains on the surface, until 2300 K is reached, and the solid surface layer begins to melt. However, the surface layer probably retains partially solid mechanical properties even beyond 2300 K, (picture g in Figure 12b). This could be due to the presence of Cr_2O_3 phases in the liquid, melting only at 2700 K.

6. CONCLUSIONS

The surface temperature of pure iron, mild steel, and stainless steel rods during the process of laser induced ignition has been tracked using adapted pyrometers, and the absorptivity at 1030 nm of the samples surface has been separately determined over time, using a photodiode in an integrating sphere. Various laser intensities (in a range from 22 to 500 $MW{\cdot}m^{-2}$) and pulse durations were used in order to assess for the influence of laser irradiation conditions on ignition.

We showed that, prior to ignition, the surface of mild steel, stainless steel, and iron rods undergoes a solid phase oxidation. When the surface temperature reaches approximately 840 K, at which FeO becomes stable and begins to form, a strong increase in the absorptivity of the surface from 0.45 to 0.7 occurs, providing more efficient energy coupling of the laser as a heat source for ignition.

The energy thresholds for ignition of iron, mild steel, and stainless steel 3.2 mm diameter samples were determined, and found to decrease with increasing laser intensity. Energy thresholds are, depending on the laser power (from 180 W to 4 kW), in a range of approximately 7 to 90 absorbed joules for pure iron and mild steel and approximately 1.5 times more than this for stainless steel.

The ignition of mild steel and pure iron is very similar in terms of temperature, except for small perturbations during a short period just prior to ignition, probably due to local ignition spots on the oxide layer, probably caused by irregularities and blisters in the solid oxide layer forming on mild steel (decarburization). Temperature measurement showed that the ignition of iron and mild steel occurs when a transition temperature of approximately 1650 K is reached, independent of laser intensity, corresponding to the melting of FeO resulting in a dramatic increase in the diffusivity of oxygen at the surface. Simple calculations based on the heat transfer equation showed that the decrease of the ignition energy threshold with increasing laser intensity could be explained by conductive thermal losses in the rod before ignition.

The ignition of stainless steel was found to be controlled by a transition temperature of approximately 1900 K, independent of the laser power used for ignition. Below this temperature, the oxide layer covering the surface retains its efficient protective properties, preventing oxidation of the underlying unoxidized steel, whereas beyond 1900 K, a steep rise of the temperature occurs, while a solid oxide remains on the surface. Ignition of stainless steel could occur when the surface reaches the melting point of magnetite Fe_3O_4, probably forming part of the solid oxide layer at the surface. Melting of Fe_3O_4 would presumably cause the oxide layer to become porous solid $FeCr_2O_4$, which melts in turn around 2300 K.

The temperature of the surface over time has been measured, and has been found to be divided in three main stages. During stage I, before ignition, the laser alone heats up the surface at relatively slow rate; during stage II, ignition occurs, and the rate of exothermic oxidation reactions increases dramatically; during stage III, the heating rate of the surface decreases, while the laser still irradiates the surface.

A 1D thermochemical model of iron ignition has been formulated and solved. Two parameters have been adjusted. The model gave results in satisfactory agreement with the experimental results, reproducing the three successive experimental stages, and gave clues to understanding the phenomena responsible for the transition between the ignition stage (stage II) and the post-ignition stage (stage III). A plausible description of the process could be stated as follows; during ignition, combustion is not limited by the diffusion of oxygen, but only by the combustion reaction itself or by the adsorption-dissociation process of oxygen at the surface, but when all the surface iron is oxidized, it is the diffusion of oxygen that becomes the rate limiting mechanism, and the reaction rate decreases.

However, our simple model failed to reproduce the persistence of the combustion observed after the end of the laser pulse. We suspect that convection movements in the melt might be responsible for a great part in the mixing of the reactants in the liquid.

ACKNOWLEDGMENTS

The second author wishes to thank Olivier Durand (ENSMA) and Olivier Marchand (ENSMA) for discussions of various issues considered in this article.

FUNDING

This work pertains to the French Government program “Investissements d’Avenir” (LABEX INTERACTIFS, reference ANR-11-LABX-0017-01) and was financially supported by Air Liquide.

REFERENCES

Abbaschian, R., Abbaschian, L., and Reed-Hill, R. 2010. *Physical Metallurgy Principles–SI Version*, 4th edition, University of California, Riverside.

Arzuov, M., Barchukov, A., Bunkin, F., Konov, V., and Luk’yanchuk, B. 1979. Combustion of metals under action of CW CO_2 laser radiation. *Sov. J. Quantum Electron.*, **9**(6), 787–789.

ASTM. 2003. G124-95: Standard test method for determining the combustion behaviour of metallic materials in oxygen-enriched atmospheres. *ASTM Standards Related to Flammability and Sensitivity of Material in Oxygen-Enriched Atmospheres*. ASTM, Philadelphia.

ASTM. 2003. ISO 14624-1—Space systems—safety and compatibility of materials, part 1: Determination of upward flammability of materials. In *Annual Book of ASTM Standards*. ASTM, Philadelphia.

Bolobov, V. 2001. Conditions for ignition of iron and carbon steel in oxygen. *Combust. Explos. Shock Waves*, **37**(3), 292–296.

Bolobov, V., Berezin, A., and Drozhzhin, P. 1991. Ignition of compact stainless-steel specimens in high-pressure oxygen. *Combust. Explos. Shock Waves*, **27**(3), 263–266.

Bolobov, V., Makarov, K., Shteinberg, A., and Drozhzhin, P. 1992. Compact-specimen burning with fresh metal-surface production. *Combust. Explos. Shock Waves*, **28**(5), 457–459.

Branch, M., Abbud-Madrid, A., Feiereisen, T., and Daily, J. 1992. A study of ignition phenomena of bulk metals by radiant heating. *J. Heat Transfer*, 265–271.

Bransford, J. 1985. Ignition of metals in high-pressure oxygen. Technical report, NASA.

Distin, P., Whiteway, S., and Masson, C. 1971. Solubility of oxygen in liquid iron from 1785 degrees to 1960 degrees C—a new technique for study of slag-metal equilibria. *Can. Metall. Q.*, **10**(1), 13–18.

Gemma, K., Kawakami, M., Kobayashi, C., Itoh, N., and Tomida, M. 1990. Kinetics of oxidation of pure iron near the eutectoid temperature of wustite. *J. Mater. Sci.*, **25**, 4555–4561.

Kirichenko, N., Morozova, E., Simakhin, A., and Nanai, L. 1989. Peculiarities of CW-CO_2 and YAG laser ignition of metals in air. *Infrared Phys.*, **29**(2–4), 427–431.

Kubaschewski, O., and Hopkins, B. 1962. *Oxidation of Metals and Alloys*. Butterworth and Co. Ltd., London.

Laurendeau, N., and Glassman, I. 1971. Ignition temperatures of metals in oxygen atmospheres. *Combust. Sci. Technol.*, **3**(2), 77–82.

Li, Y., Fruehan, R.J., Lucas, J.A., and Belton, G.R. 2000. The chemical diffusivity of oxygen in liquid iron oxide and a calcium ferrite. *Metall. Mater. Trans. B*, **31**(5), 1059–1068.

Lide, D. R. 2007. *CRC Handbook of Chemistry and Physics*., CRC Press, Boca Raton, FL.

McIlroy, K., Zawierucha, R., and Drnevich, R. 1988. Promoted ignition behavior of engineering alloys in high pressure oxygen. In *Flammability and Sensitivity in Oxygen-Enriched Atmospheres: Third Volume, ASTM STP 986*, D. W. Schroll (Ed.), American Society for Testing and Materials, West Conshohocken, PA, pp. 85–104.

Mellor, A. 1967. Heterogeneous ignition of metals: Model and experiment. Technical report 816, NASA.

Moreau, J. 1953. Étude du mécanisme de l'oxydation des alliages binaires fer-chrome aux tempratures élevées. *C. R. Acad. Sci.*, **236**, 85–87.

Muller, M., Fabbro, R., El-Rabii, H., and Hirano, K. 2012. Temperature measurement of laser heated metals in highly oxidizing environment using 2D single-band and spectral pyrometry. *J. Laser Appl.*, **24**(2), 022006.

Neary, R. 1983. ASTM G60: A milestone in a 60-year safety effort. In *Flammability and Sensitivity in Oxygen-Enriched Atmospheres: Third Volume, ASTM STP 812*, American Society for Testing and Materials, West Conshohocken, PA.

Nguyen, K., and Branch, M. 1987. Ignition temperature of bulk-6061 aluminum, 302-stainless steel and 1018-carbon steel in oxygen. *Combust. Sci. Technol.*, **53**(4–6), 277–288.

Office technique pour l'utilisation de l'acier (France). 1995. *Données physiques sur quelques aciers d'utilisation courante*. Aciers français. OTUA, Paris-la-Défense.

Ryschkewitsch, M. 1998. Flammability, odor, offgassing, and compatibility requirements and test procedures for materials in environments that support combustion, test 17, upward flammability of materials in gox. NASA-STD-6001. NASA, Washington, DC.

Sato, J., Ohtani, H., and Hirano, T. 1995. Ignition process of a heated iron block in high-pressure oxygen atmosphere. *Combust. Flame*, **100**(3), 376–383.

Sato, J., Sato, K., and Hirano, T. 1983. Fire spread mechanisms along steel cylinders in high pressure oxygen. *Combust. Flame*, **51**, 279–287.

Seban, R. 1965. Emissivity of transition metals in infrared. *J. Heat Transfer*, **87**(2), 173–176.

Seibold, G., Dausinger, F., and Hugel, H. 2000. Absorptivity of Nd: YAG-laser radiation on iron and steel depending on temperature and surface conditions. In *Icaleo(r) 2000: Proceedings of the Laser Materials Processing Conference*, **89**, 125–132.

Shen, G., Lazor, P., and Saxena, S. 1993. Melting of wustite and iron up to pressures of 600 kbar. *Phys. Chem. Miner.*, **20**(2), 91–96.

Steinberg, T., M. Rucker, and H. Beeson 1989. Promoted combustion of nine structural metals in high-pressure gaseous oxygen: A comparison of ranking methods. *American Society for Testing and Materials, STP. Flammabl. Sensit. Mater. Oxyg.-Enrich. Atmos. 1040*, 54–76.

von Grosse, A., and Conway, J. 1958. Combustion of metals in oxygen. *Ind. Eng. Chem.*, **50**(4), 666–672.

Wilson, D., Steinberg, T., and Stolzfus, J. 1997. Thermodynamics and kinetics of burning iron. In *Flammability and Sensitivity in Oxygen-Enriched Atmospheres: ASTM STP 1319*, American Society for Testing and Materials, West Conshohocken, PA, pp. 240–257.